ASCE

Optimization of Hydraulic Fracture Treatment Parameters for Normally Pressured Longmaxi and Wufeng Shales in the Southeastern Sichuan Basin in China

Melckzedeck M. Mgimba[1]; Shu Jiang[2]; and Wilson Ngole[3]

Abstract: Lower Silurian Longmaxi and Upper Ordovician Wufeng shales are gas-producing formations. These formations have ultralow porosity and permeability in the southeastern Sichuan Basin and have normal formation pressures with pressure coefficients of less than 1.2. Hydraulic fracturing has been proven as the best development strategy to produce gas. But choosing hydraulic fracture treatment parameters becomes challenging due to strong reservoir heterogeneity, significant horizontal stress contrast and high in situ stress in this region. We employed the pseudo-three-dimensional (P3D) model to study fracturing fluid types, injection rates, and proppant sizes to optimize the fracturing design of these shale formations. First, this model was solved in the simulator by the finite element method (FEM) to obtain the fracture height, length, and width. Then the results were validated by 3D Tip dominated model, and the perkins-kern-nordgren (PKN) and khristianovic-geertsma-deklerk (KGD) analytical models, which are popular and most used in designing hydraulic fractures. It was found that as the volumetric injection rate and gel loading in the fracturing fluid rise, so do the generated fracture length and width. Furthermore, the formations' stress contrast affected the shape of the fracture, the interval with lower stress had a wider fracture compared to the interval with higher stress. Also, the higher stress in the layers above and below the shale formations contained the fracture height, which favored the growth of fracture in the shale formations. Lastly, it is suggested that a fluid with gel loading of 60 ppgt, proppant with 12/20 mesh size and an injection rate of 6.36 m^3/min be used in these shale formations with normal reservoir pressure. These parameters' combinations created the most extended propped fracture length of 264.8 m, and the average width was 1.06 cm. **DOI: 10.1061/JLEED9.EYENG-4494.** © *2023 American Society of Civil Engineers.*

Introduction

In the current years' gas from shale formation has become very important to global energy (Guo et al. 2021; Liu et al. 2022). America's success in developing and producing shale gas formations raises the understanding of exploring and producing shale gas in the world. China is among the countries with huge potential for shale gas and is looking forward to replicating the US (Jiang et al. 2016a). One field that contains shale gas formations in China is the Fuling gas field found in the Eastern Sichuan Basin. The field has a gas reserve of 7.68516×10^{11} m^3 and is claimed to be one of the world's most significant shale gas deposits (Dai et al. 2017; Jiang et al. 2016b; Wang et al. 2021a). Among the shale gas formations in the Fuling gas field are Lower Silurian Longmaxi and Upper Ordovician Wufeng Formations. These shale gas formations have a pressure coefficient of less than 1.2 and ultralow porosity and permeability; thus, they are tight formations (Wang et al. 2021a). Due to the tightness of these formations, the conventional way of developing these formations to obtain gas becomes difficult. Based on Ahmed et al. (2019), Aminzadeh (2018), Cui et al. (2022), Sadrpanah et al. (2006), and Xie et al. (2022), hydraulic fracturing seems to be a feasible development strategy for these kinds of formations. According to Society of Petroleum Engineers (2012), propped hydraulic fracturing provides better production when used in 0shale formations, and this is because propped hydraulic fracturing is capable of creating long fractures and keeping the fracture open after fracturing. These significances suggest the propped hydraulic fracturing in the Lower Silurian Longmaxi and Upper Ordovician Wufeng Shale Formations in the southeast of the Sichuan Basin.

The models used in designing the hydraulic fracture are grouped into two-dimensional (2D) and three-dimensional (3D) models (Muther et al. 2020). The most common 2D models used are the Perkins-Kern-Nordgren (PKN) and Khristianovic–Geertsma–de Klerk (KGD) (Geertsma and Haafkens 1979; Muther et al. 2020; Nguyen et al. 2020, 2022; Zolfaghari et al. 2017). According to Esfandiari and Pak (2022), these 2D models were the first and most used analytical models. However, in these models, the fracture height is assumed to be constant. Therefore, these models are not good at approximating lateral and vertical fracture propagation in hydraulic fracturing (Wong 2018).

The pseudo-three-dimensional models (P3D) were developed to mitigate the problem of 2D models and were the first 3D models to be used in multilayered reservoirs (Muther et al. 2020). These models are characterized by elliptical or lumped models (Adachi et al. 2007) and cell-based models (Settari and Cleary 1986). In elliptical models, the shape of a fracture is an ellipse with two half-ellipses connected at the center. In contrast, no specific shape is defined for the cell-based models. These models are the modification of PKN,

[1]Ph.D. Candidate, Key Laboratory of Tectonics and Petroleum Resources of Ministry of Education, Key Laboratory of Theory and Technology of Petroleum Exploration and Development in Hubei Province, China Univ. of Geosciences, Wuhan 430074, China; Dept. of Geosciences and Mining Technology, Mbeya Univ. of Science and Technology, P.O. Box 131, Mbeya 53119, Tanzania (corresponding author). ORCID: https://orcid.org/0000-0003-3670-7094. Email: melckmgimba1@gmail.com

[2]Professor, Key Laboratory of Tectonics and Petroleum Resources of Ministry of Education and Key Laboratory of Theory and Technology of Petroleum Exploration and Development in Hubei Province, China Univ. of Geosciences, Wuhan 430074, China. Email: jiangsu@cug.edu.cn

[3]Dept. of Geosciences and Mining Technology, Mbeya Univ. of Science and Technology, P.O. Box 131, Mbeya 53119, Tanzania. Email: wile.ngole@gmail.com

Note. This manuscript was submitted on March 3, 2022; approved on November 29, 2022; published online on January 30, 2023. Discussion period open until June 30, 2023; separate discussions must be submitted for individual papers. This paper is part of the ***Journal of Energy Engineering***, © ASCE, ISSN 0733-9402.

whereby the fluid flow and fracture heights are evaluated from the pressure in the cell (Adachi et al. 2007; Guo et al. 2007). The P3D model works better for fractures where the length-to-height ratio is more significant (Palmer and Craig 1984). However, this model is not recommended for unstable fracture height growth formations.

The propagation of hydraulic fractures depends on the reservoir properties, such as permeability, reservoir temperature, porosity, reservoir depth, and initial reservoir pressure. Also, fracture growth depends on the mechanical rock properties, including horizontal principal stress, toughness, Poisson's ratio, closure stress gradient, Young's modulus, and average fracture pressure gradient. The fractures grow in a complex manner due to these properties. Hence, selecting an appropriate model to be used in designing hydraulic fracturing is necessary.

The hydraulic fracturing fluid types, proppants sizes and injection rates are among the essential parameters during hydraulic fracturing treatment design. The hydraulic fracturing fluid is used to carry the fracturing energy to break the rock and take the proppants to the fracture open (Ghahremani and Clapp 2014). The application of hydraulic fracturing fluids depends on several factors, including the nature and lithology of formation, fluid in the formation, cost and proppants' carrying ability (Haddad et al. 2017; Montgomery 2013; Parekh and Sharma 2004). For instance, water is not recommended as a fracturing fluid in some formations due to its ability to form water drops in the gas formation and swelling effects in the clay minerals. These two factors reduce the relative permeability of reservoir fluids (Haddad et al. 2017; Parekh and Sharma 2004). Studies conducted by (Barati and Liang 2014), Da et al. (2022), and Wrobel et al. (2021) revealed that high-viscous fracturing fluid has a high ability to carry a high concentration of proppants to the fracture and create a wide and short fracture. But Da et al. (2022) noted that high-viscous fracturing fluid has low flowback efficiency, thus damaging the reservoir by retaining fracturing fluid in the fracture matrix zone. Da et al. (2022), on the other hand, demonstrated that using low-viscosity fluid can also damage the reservoir because it can be trapped in the tiny pores of the reservoir.

Proppants are chosen for hydraulic fracturing based on their size, strength, cost, the reservoir permeability or conductivity they induce, and the minimum in situ stress (closing stress) of the formation (Chamanzad et al. 2017; Economides and Nolte 1989). The size of the proppants can be measured by mechanical sieve analysis or hydrometer. The standard way of presenting the size of the proppants is using the mesh size range, as shown in Table 1. According to Olmen et al. (2018), the proppants with 100, 40/70, and 20/40 mesh sizes are widely used in the hydraulic fracturing process for sealing the micro-cracks (100 mesh size) and holding the fracture open.

Mathematical relation [Eq. (1)] shows that the settlement velocity of the proppants is directly proportional to the square of the diameter of the proppants (Belyadi et al. 2019). Thus, the large-size proppant needs a higher injection rate to avoid earlier settlement of the proppants

$$V_{se} = \frac{g(\rho_{pr} - \rho_{fl})d_{pr}^2}{18\mu_{fl}} \quad (1)$$

where V_{se} = settling velocity of the proppants; g = acceleration due to gravity; ρ_{pr} = density of the proppant; ρ_{fl} = density of the fluid; d_{pr} = proppant diameter; and μ_{fl} = viscosity of the fluid.

Based on Bokane et al. (2013), Guo et al. (2022), and Siddhamshetty et al. (2020), proppants of small sizes are well transported and distributed in multistage fractures and can be carried to a more extended fracture when compared to large-size proppants. But the earlier settlement of proppants (proppants carried to a shorter fracture) can also be caused by a low flowing rate below the critical settling velocity, the low viscosity of fracturing fluid and higher proppant density (Da et al. 2022; Huang et al. 2019; Montgomery 2013). From these studies, the authors suggested evaluating the proper values of hydraulic fracturing parameters, including viscosity, injection rate and concentration of proppant, by balancing them is important to obtain a more extended propped fracture.

The studies conducted in the southern Sichuan Basin by Cao et al. (2020) and Liu et al. (2021) showed that the shale formations have substantial reservoir heterogeneity, significant horizontal stress contrast and high in situ stress. These factors led to problems during proppants placement, fracture growth, and production variation after hydraulic fracturing. Thus, the studies suggested high injection rate, high viscous fracturing fluid, low density and small-sized proppants to mitigate those problems. But the study does not show the quantity of these suggested parameters. Duan et al. (2019) studied the hydraulic fracturing techniques in the Dingshan area in the southeastern Sichuan Basin, which is analogous to our study area. In that study, the method of horizontal well fracturing in deep formations was developed. Three wells (Well DY2, Well DY4, and Well DY5) were tested in that developed method. The high viscous slick water was used as a fracturing fluid in all wells, the injection rates were 12, 16, 18 m^3/min for Well DY2, Well DY4, Well DY5, respectively. And the size of proppants used were 40/70 and 30/50 mesh sizes for sealing the wall and holding the fracture open. These parameters show success in production, but in this study, the fracturing parameters were not varying. Studying of various fracturing parameters like different fracturing fluid types, different injection rates, and various proppants sizes could bring more successful results.

Even though Bokane et al. (2013), Da et al. (2022), and Huang et al. (2019) showed the effect of each fracturing parameter (fluid type, proppants size, and injection rate), these studies did not show the impact of the combination of these fracturing parameters in the southeast of Sichuan Basin. Likewise, Cao et al. (2020) and Duan et al. (2019) did not show the impact of each of these fracturing parameters on developing the fracture. Also, we found that the process of choosing appropriate fracturing fluids, proppants size, and injection rate during the hydraulic fracturing process is very challenging. Due to this research gap, this study will focus on studying fracturing fluid type, injection rate, and proppants size through the simulations. Then, the study will suggest the fracturing fluid, its injection rate, and the size of the proppants to be used during the hydraulic fracturing process in the Lower Silurian Longmaxi and Upper Ordovician Wufeng shales in the southeast of the Sichuan Basin.

To reach the study's goals, we used a unique P3D model called the 3D shear decoupled method to evaluate fracture growth. But the results were validated by PKN, KGD and another P3D model called 3D tip-dominated model. According to Chen et al. (2019), the PKN

Table 1. Proppants size distribution

Mesh size	Particle size range ($\times 10^{-6}$ m)
10/14	1,400–2,000
12/20	850–1,700
16/20	850–1,180
16/30	600–1,180
20/40	420–850
30/50	300–600
40/70	212–420
100	149

Source: Data from Lutynski (2015).

and KGD models can validate the fracture simulation results for short and long simulation times. Also, Rahman and Rahman (2010) commented that these 2D models are the most popular. The 3D tip-dominated model considers the influence of extreme permeability contrast layers. In this case, the hydraulic fracture growth can be arrested due to increased fluid leak-off as the hydraulic fracture tip enters a high-permeable layer.

Geological Setting

The study was conducted in the southeastern Chongqing region, which is found on the boundary of the southeastern Sichuan Basin, as shown in Fig. 1. The Sichuan Basin is located in the southwest of China and is part of the Yangtze Platform found in Northwestern (Li et al. 2022; Zhou et al. 2021). It is a giant, intracratonic basin on

Fig. 1. Distribution of shales in China, showing the study area. [Reprinted from *Natural Gas Industry B*, Vol. 3(1), D. Dong, Y. Wang, X. Li, C. Zou, Q. Guan, C. Zhang, J. Huang, S. Wang, H. Wang, H. Liu, W. Bai, F. Liang, W. Lin, Q. Zhao, D. Liu, and Z. Qiu, "Breakthrough and prospect of shale gas exploration and development in China," pp. 12–26, © 2016, with permission from Elsevier.]

the stable South China Block. The coverage of the Sichuan Basin is about 23×10^{10} m^2, and in 2014 the basin had a proven gas reserve of about 3.22×10^{12} m^3. The basin was formed in the late Proterozoic and extended to the present day (Korsch et al. 1991; Liu et al. 2017). In the middle of the basin, the basement contains transitional basite magmatic rocks that have experienced intense metamorphism (Luo 1998).

Various formations were formed in the southeast of Chongqing during the Cambrian, Ordovician and Silurian ages, whereas other formations are missing due to tectonic uplift and erosion.

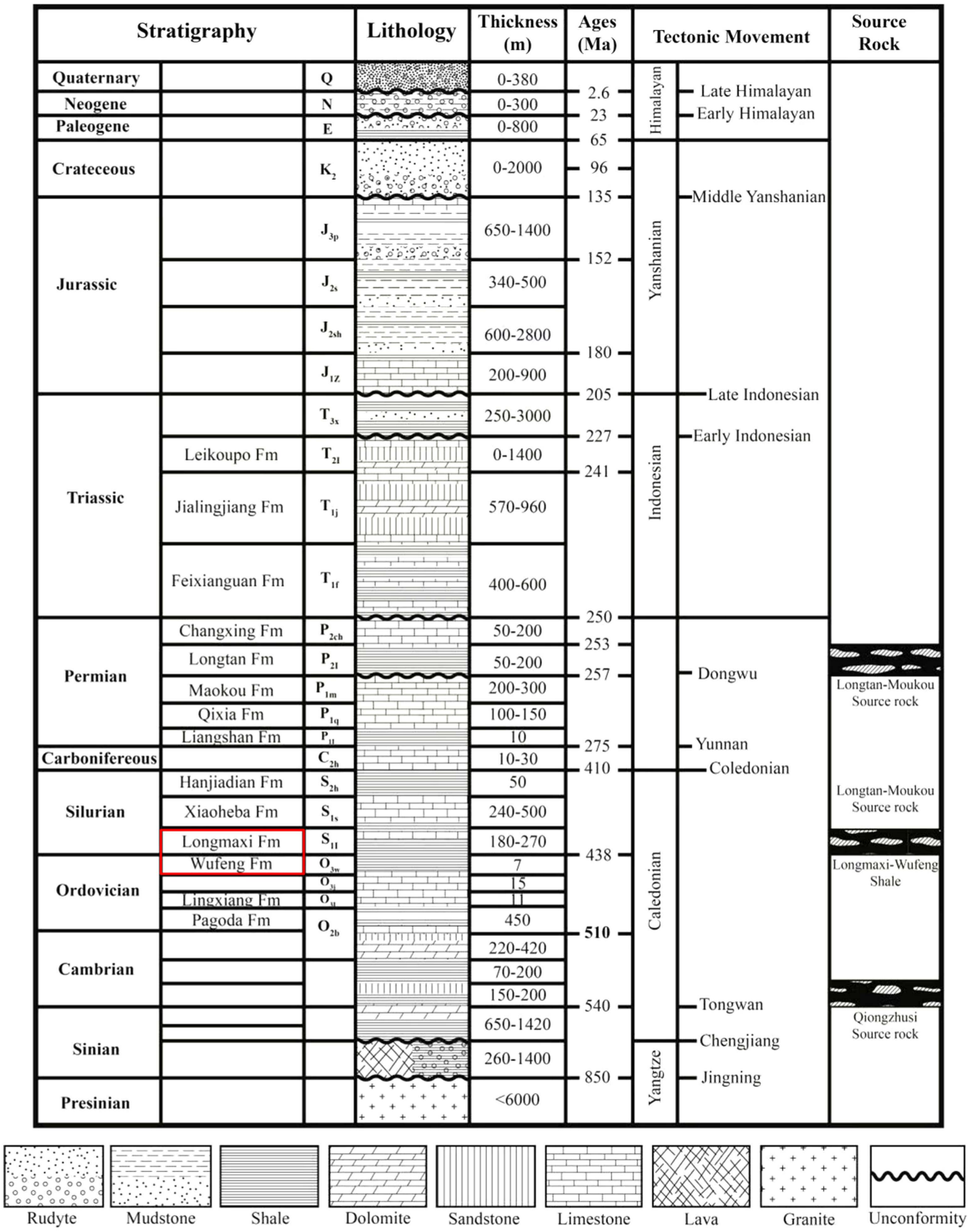

Fig. 2. Stratigraphy of the southeastern Chongqing region showing Longmaxi and Wufeng formations. [Reprinted from Wang et al. (2021b), under Creative Commons-BY-4.0 license (https://creativecommons.org/licenses/by/4.0/).]

J. Energy Eng., 2023, 149(2): 04023004

The primary source rocks in the area are Lower Cambrian Niutitang Formation, Lower Silurian Longmaxi Formation and Upper Ordovician Wufeng Formation, as shown in Fig. 2 (Li et al. 2022; Wang et al. 2021a, b). The Longmaxi and Wufeng shales are the primary targets for exploring and developing shale gas in the southeast of Chongqing area. These formations are rich in organic matter, have high thermal alteration, and are deep in depth. The main conditions influencing high shale gas production in these formations were accelerated by the stable anaerobic environment, which occurred for a long time (Wang et al. 2021a).

Pengye 1 is one of the wells drilled to evaluate the Longmaxi and Wufeng shales gas reservoirs. The well shows that the shale region is divided into three parts, top, middle, and bottom. The top part starts from a depth of 2,010 to 2,055 m and contains gray limestone, shale and shale sandstone. The central part starts from a depth of 2,055 to 2,122 m and has gray shaly sandstone, gray and black mudstone. Finally, the bottom part starts at a depth of 2,122 to 2,160 m and contains gray and black carbonaceous shale and mudstone. The well shows the Longmaxi shale is found at a depth between 2,072 and 2,152 m, whereas the Wufeng shales are located at a depth between 2,152 and 2,160 m (Chen et al. 2018; Mgimba et al. 2022).

The exploration shows that the pressures in these shale formations range from under to normal pressure (the average formation pressure coefficient is 1) (Mgimba et al. 2022; Nie et al. 2017). Both formations are tight formations and have ultralow porosity and permeability. According to Wang et al. (2021a), the average porosity of Wufeng-Longmaxi shale in the southeast of Chongqing area is 1.25%, while the average permeability of 72.1% of the studied region is about 1×10^{-7} Darcy (D). The area was squeezed in the Early to Middle Jurassic and formed several thrust faults (Zhang et al. 2018). The stress regimes of the thrust faults changed from extrusion to extension during the Cretaceous but due to the influence of the intrusion of the India-Australian plate onto the Eurasian plate, the stress regime altered again from extension to extrusion during the Neogene (Wo et al. 2007). Therefore, the region comprises several natural fractures orienting in NW-SE, NE-SW, NWW-SEE, and NEE-SWW directions.

Methodology

The study of fracturing fluids, proppant sizes and injection rates during hydraulic fracturing in this work was done through the simulation method. It was assumed that design calculations represent actual and quantitative fracture behavior. The work passes through different stages, including; data collection, selecting the fracture model to be used in the simulator, fracturing fluid selection, selection of the proppants and selection of optimum injection rate, as shown in Fig. 3. Then the effect of stress contrasts was studied and validation of the results was done.

Selection of Hydraulic Fracture Model

The FracPro 2019 simulator was used in this work to analyze fracture growth. But according to Azad et al. (2022), the FracPro 2019 simulator is developed based on the P3D model. According to Adachi et al. (2010) and Shel and Paderin (2019), the main assumption in the P3D model are uniform minimum in situ stress, the fracture is growing in elliptical or cell-based, fluid leak-off is treated based on Carter's model, and also it exists a condition of plane strain in any vertical plane. The development of fracture by the P3D model is governed by Eqs. (2) and (3) from the shape of the fracture (elliptical). Also, the model considers the relationship

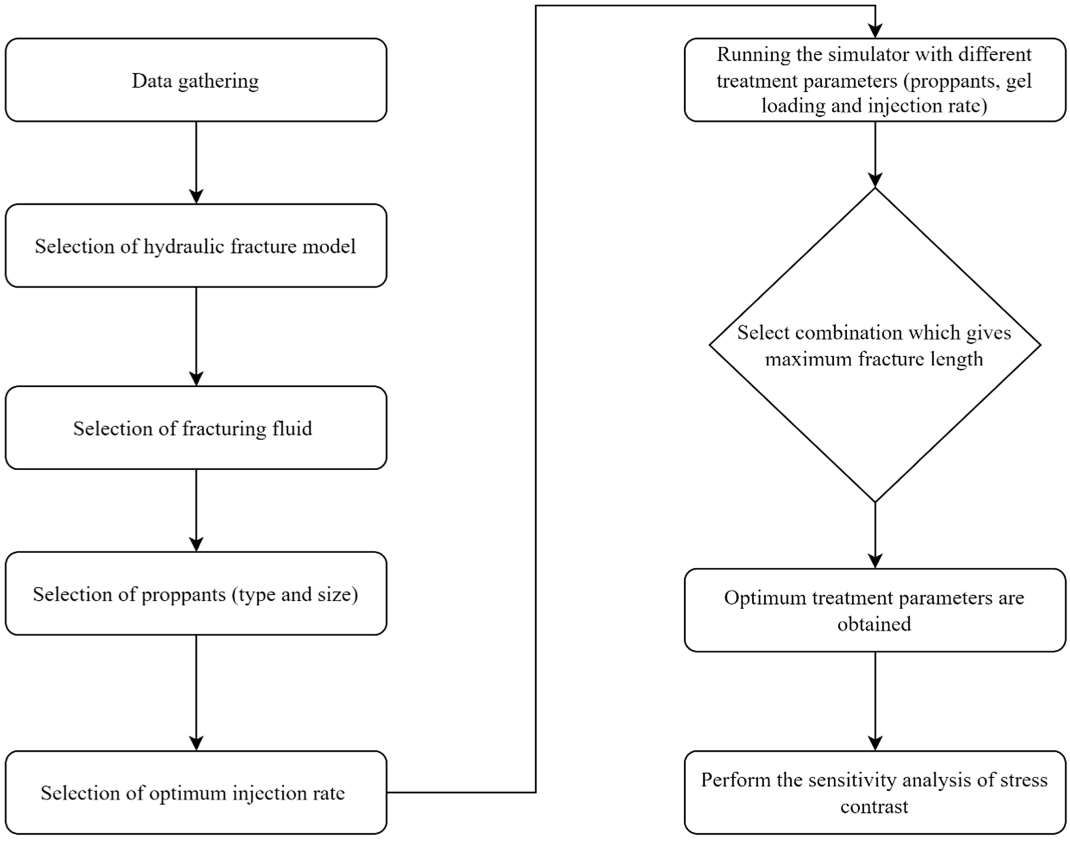

Fig. 3. Stages followed to obtain the optimum treatment parameters.

between fracture development and net pressure, Poiseuille's law, and the law of conservation as described by Eqs. (4), (6), and (7), respectively. During the simulation, the simulator considers the boundary conditions as shown by Eqs. (5) and (6) (Adachi et al. 2010; Shel and Paderin 2019)

$$\bar{w} = \frac{1}{H}\int_{-h/2}^{h/2} w dz \tag{2}$$

$$\bar{q} = \frac{1}{H}\int_{-\frac{h}{2}}^{\frac{h}{2}} q dz \tag{3}$$

where $\bar{w}$ = average width; $\bar{q}$ = average flow rate; H = reservoir height; and h = equilibrium height.

The relationship between fracture development and the net pressure was developed from the elasticity. This relation is represented by the integral equation of fracture width [Eq. (4)] and stress intensity factor [Eq. (5)], both in the form of net crack loading

$$w = \frac{4}{\pi \bar{E}} p \int_0^{H/2} GK(s,z) ds + (p - \Delta\sigma)\int_{H/2}^{h/2} GK(s,z) ds \tag{4}$$

$$K_I = \sqrt{\frac{8h}{\pi}}\left[p\int_0^{H/2} \frac{ds}{\sqrt{h^2 - 4s^2}} + (p - \Delta\sigma)\int_{H/2}^{h/2} \frac{ds}{\sqrt{h^2 - 4s^2}}\right] \tag{5}$$

where $\bar{E}$ = plane strain Young's modulus; p = net pressure; and GK(s,z) = elasticity kernel.

The relationship between the flow rate (average flux) and the pressure gradient is defined by Poiseuille's law [Eq. (6)]

$$\frac{\partial \bar{q}}{\partial x} = \frac{w^3}{12\mu}\frac{\partial p}{\partial x}, \qquad -\frac{h}{2} < z < \frac{h}{2} \tag{6}$$

Also, the law of conservation defined by Eq. (7) is considered

$$\frac{\partial \bar{q}}{\partial x} + \frac{\partial \bar{w}}{\partial x} + \frac{C}{\sqrt{t - t_o(x)}} = 0 \tag{7}$$

where $t_o(x)$ = time the crack reaches coordinate x, and C Carter leak-off coefficient.

In the simulator, the following boundary conditions are used [Eqs. (8) and (9)]

$$\bar{w}(l,t) = \bar{q}(l,t) = 0, \qquad h(l,t) = H \tag{8}$$

$$q(0,t) = \frac{Q_0}{2H} \tag{9}$$

where l = length of the fracture; and t = time required to create the fracture.

Based on Cipolla and Wright (2000), Huo et al. (2021), and Muther et al. (2020), the shale formations which are sandwiched by limestone lithologies tend to develop a confined fracture due to high-stress contrast. This mechanism favors the fracture to have a higher length when compared to height. As Longmaxi and Wufeng shale formations in the southeastern Sichuan Basin exhibit this behavior, the 3D shear decoupled model provided by the FracPro 2019 simulator has been selected to be used. The model has been used since it considers the formation response to confined stress. This model is a kind of P3D approximating a more confined and longer hydraulic fracture caused by the composite layering effect. This confinement phenomenon and fracture growth behavior cannot be precisely evaluated through 2D analytical models since they can provide smaller or larger fracture geometry values than reality.

The P3D model is solved by the Finite Element Method (FEM) in the FracPro 2019 simulator. FEM is an algorithm for solving partial differential equations in two or three spatial variables [for instance, Eqs. (6) and (7)]. The FEM breaks down a complex system (fluid pressure, stress in rock, fluid flow rate and width relation) into smaller, more manageable pieces known as finite elements to solve an issue. The numerical domain for the solution, which has a finite number of points, is implemented by creating a mesh of the object using a specific space discretization in the space dimensions. A set of algebraic equations emerges from formulating a boundary value problem using the finite element approach. The technique makes domain-wide approximations of the unknown function. The small system of equations that describes these finite elements is then combined with other equations to model the full issue. Then Gaussian elimination method is used to find a solution (Annigeri and Cleary 1984; Wangen 2011; Wangen 2013).

The Description of the Reservoir

The formations used in this work consist of shale lithology. The pay zone is found in Longmaxi and Wufeng shales, located at a depth between 2,072 and 2,160 m. Most reservoir properties were obtained from the East China Branch of Sinopec Co., Ltd. report, which conducted the exploration. Other data, including porosity and permeability, were obtained from the literature (Wang et al. 2021a), and a few data were assumed from experience, as shown in Table 2. According to Wang et al. (2021a), the porosity in this area ranges from 0.05% to 5.61%, with an average of 1.25%. Since the porosity at different depths was not present, the average porosity was used in this work. Also, the permeability in these formations ranges from 5×10^{-10} to 1.626×10^{-7}D, whereas the average permeability of 72.1% of the region is about 1×10^{-7}D. Therefore, the permeability of 1×10^{-7}D was used in the simulation. There is a variation of porosity and permeability in these formations, but generally, the formations show ultralow porosity and permeability. Other reservoir parameters in these formations are shown in Table 2.

Other important parameters to be considered in the reservoir are the mechanical properties of the rock. The mechanical properties of the rock are critical parameters to be considered in hydraulic fracturing. These properties influence the size and geometry of the fractures developed during the hydraulic fracturing process. These properties were obtained from the report of the East China Branch of Sinopec Co., Ltd. Most of the rock mechanics' properties change with depth, as shown in Fig. 4, where the Young's modulus and Poisson's ratio vary with depth in the same formation. Inside the shale formations, there was also fluctuation in the magnitude of stress at different levels, which had an impact on the shape of the fracture. Additionally, the layer above and below the shale formations has a difference in stress, which affects the fracture height growth. When there is higher stress above and below the zone of

Table 2. Reservoir data of Longmaxi and Wufeng shales which were used for fracture design

Parameter	Unit	Value	Citation
Average reservoir pressure	Pa	23.88×10^6	Data from the report
Static reservoir temperature	°C	61	Chen et al. (2018)
Porosity	%	1.25	Wang et al. (2021a)
Reservoir thickness	m	88	Data from the report
Permeability	D	1×10^{-10}	Wang et al. (2021a)
Water saturation	%	20	Assumed
Total compressibility	1/Pa	5.63×10^{-8}	Wang et al. (2021a)

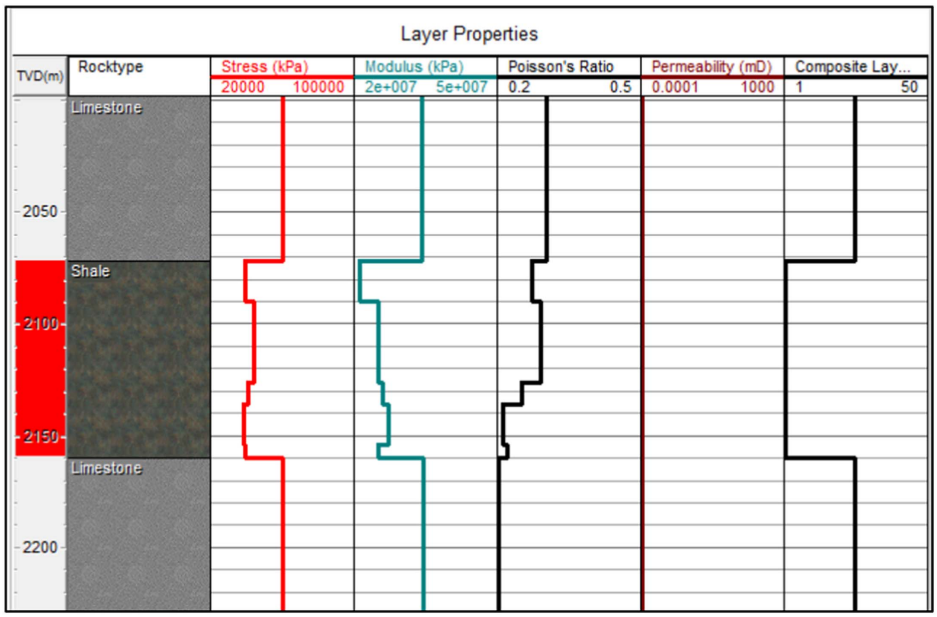

Fig. 4. Rock mechanics properties of the Lower Silurian Longmaxi and Upper Ordovician Wufeng shales in the southeastern Chongqing area, these properties were included in designing the fractures.

interest, the increase of the fracture height is restrained (Long and Xu 2017). It was therefore assumed that these strata had higher stress (60 MPa) than the relevant shale formations for a fracture to appear in the shale formations and for the study to concentrate on width and length expansion. Also, the mechanical properties of the rock are required for predicting the closure stress gradient, which helps in approximating the injection pressure needed to break the rock and create a fracture. Therefore, the simulator used the reservoir and the rock's mechanical properties to model the reservoir.

The Wellbore Configuration

The hydraulic fracturing process was done in the horizontal well. The horizontal well has many advantages in the petroleum industry, including having a large contact area with the formation, higher productivity, and stability to stresses acting on them (Soliman et al. 1990; Xie et al. 2022). The fractures are developed when the hydraulic fracturing fluid is pumped at high pressure through the horizontal well to the perforated region, as shown in Fig. 5 (Zuppann and Steinmetz 2014). According to the fracture development, the length of the fracture should increase in step with the formations while the height of the fracture should cross perpendicular to them. The FracPro 2019 simulator was used to model the fractured horizontal well, with a measured length of 4,000 m. The vertical section had a length of 2,100 m, and the horizontal section had a length of 1,900 m. Then, the well was perforated from a length of 2,100 to 4,000 m. In this well, a single fracture was developed to optimize the hydraulic fracture treatment parameters (fluid type, fluid viscosity, proppant size, and injection rate).

The Selection of Fracturing Fluid

The selection of fracturing fluid depends on technical factors and economic factors. Among the main technical factors considered in the selection of fracturing fluid are the loss in fluid viscosity and friction, gel damage and compatibility with the reservoirs (Abaa et al. 2012). Therefore, considering technical factors is necessary for controlling wellbore damage, fracture development, and proppants carrying. The economic factors are considered when the technical factors meet the requirement. This work mainly concentrates on two technical aspects, the fracturing fluid viscosity and its compatibility with the formation.

Fracturing Fluid Viscosity

The fluid viscosity has two impacts on the fracture created; first, it affects both fracture length and width and second, it affects the proppants distribution in the fracture. High viscous fracturing fluid creates wide fractures and increases the ability to carry a high proppant concentration. In contrast, low viscous fluid has a low ability to carry proppants and create thin fractures, but its advantage is low cost and easy availability. According to Gidley (1989), proppants

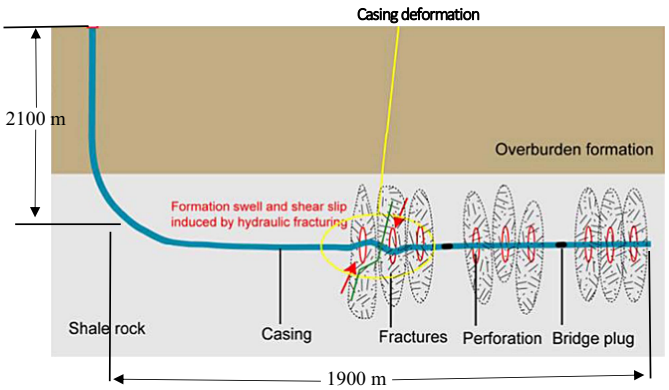

Fig. 5. Sketch of the horizontal well in which fracturing fluid was pumped to initiate the fracture, the vertical section length was 2,100 m, and the horizontal section length was 1,900 m. (Reprinted from *Journal of Petroleum Science and Engineering*, Vol. 166, F. Yin, L. Han, S. Yang, Y. Deng, Y. He, and X. Wu, "Casing deformation from fracture slip in hydraulic fracturing," pp. 235–241, © 2018, with permission from Elsevier.)

will be suspended in the fracture if the fluid viscosity in the fracture range from 50 to 100 cp. After sometimes, the fluid will lose its viscosity to allow proppants to settle before the fracture close. Thus, the fluid should be able to suspend the proppant and send them into the fracture, but also it should lose viscosity after some time to allow the proppants to settle in the fracture. Different fracturing fluids were simulated to evaluate their ability to develop fractures and distribute proppants.

Reservoir Compatibility

The choice of fracturing fluid depends on the sensitivity of the reservoir to that fluid and its additives. Therefore, considering fluid sensitivity in a specific reservoir is necessary for selecting fracturing fluid. For example, a reservoir which contains clay minerals is very sensitive to water (Parekh and Sharma 2004). Therefore, using water-based-fracturing fluid causes clay swelling in a reservoir, which blocks the wellbore that is not stable, causing stuck pipe and destruction of fracture by the movement of fine particles. Therefore, adding additives like KCl, which reduces clay's swelling, is required if water is selected for this kind of reservoir. Otherwise, other fracturing fluids that prevent clay minerals' swelling are necessary for these reservoirs. The problem of clay swelling was discovered in this reservoir because some layers are shale formations that contain clay minerals. Thus, fracturing fluid was selected by considering the clay swelling factor.

Injection Rates

The performance of fracturing fluid in creating the fractures depends on the injection rate. Therefore, the effect of different injection rates was evaluated in this work. Based on Abaa et al. (2012), the maximum injection rate due to the limitation of the pump is 100 bpm (15.90 m^3/min). However, the injection rates used in this work range from 1.59 to 15.90 m^3/min due to the injection rate's capacity to induce fracture.

Selection of Proppants and Study of the Effect of Proppant Sizes

The proppant type choice depending on the formation's closure stress is shown in Table 3. The Beta factor affects the non-Darcy pressure drop in the fracture. The smaller value of the Beta factor diminishes non-Darcy pressure drops in the fracture (Al-Sadhan 2014). Thus, it causes an improved conductivity, resulting in an enhanced flow rate and production of hydrocarbons. The cost of proppants is another essential factor in considering the proppants to be used. The cost includes transportation costs, buying or preparing proppants, and their availability. According to Liang et al. (2016), sand is the cheapest and most common proppants.

The closure stress in this formation is 3.7838×10^7Pa (5,488 psi), according to Belyadi et al. (2019) and Cholet (2008); sand proppants can be applicable in these formations with closure stress less than 4.1×10^7Pa. Therefore, sand proppants from Arizona were selected based on the cost and the good performance of sand proppants at closure stress of less than 4.1×10^7Pa. The proppants are found in different mesh sizes ranging from 100 to as large as 10/20 mesh size. In this work, three proppants types (I2/20, 20/40, and 40/70 mesh sizes) were selected for the study because they are commonly used in the petroleum industry. The permeabilities of these proppants at a closure stress of 3.7838×10^7Pa are shown in Table 4.

Table 3. The application of proppants at different closure stresses

Proppant	Specific gravity	Maximum closure stress ($\times10^7$Pa)
Sand	2.65	4.1
Resin-coated sand	2.55	6.9
ISP ceramics	2.7–3.3	9.7
High-strength proppant	3.4	>6.9

Source: Data from Cholet (2008).

Table 4. Proppant with 12/20, 20/40, and 40/70 mesh sizes used in the study with their permeabilities at a closure pressure of 3.7838×10^7 Pa

Proppant types	Proppant size	Proppant permeability (D)
Arizona sand	I2/20	367.40
Arizona sand	20/40	85.78
Arizona sand	40/70	31.17

Methods of Validating the Results

In validating the results, KGD and PKN models were used. The KGD analytical solutions which were used in the validation of the results are shown in Eqs. (10) and (11) (Nordgren 1972; Zielonka et al. 2014)

$$L = 0.11\left(\frac{8q_o^3G}{(1-v)\mu}\right)^{\frac{1}{6}}t^{\frac{2}{3}} \tag{10}$$

$$W_{max} = 0.15\left(\frac{(1-v)q_o^3\mu}{G}\right)^{\frac{1}{6}}t^{\frac{1}{3}} \tag{11}$$

where L = fracture length (m); q_o = injection rate (m^3/s); G = shear modulus (Pa); μ = fracturing fluid viscosity (Pa.s); H = fracture height (m); W_{max} = maximum width; and t = time (s).

The PKN analytical solution, which did not consider the fluid leak-off, is shown by Eqs. (12) and (13) (Nordgren 1972)

$$L = 0.39\left(\frac{q_o^3G}{\mu H^4}\right)^{\frac{1}{5}}t^{\frac{4}{5}} \tag{12}$$

$$w_{max} = 2.17\left(\frac{q_o^2\mu}{G.H.}\right)^{\frac{1}{5}}t^{\frac{1}{5}} \tag{13}$$

where L = fracture length (m); q_o = injection rate (m^3/s); G = shear modulus (Pa); μ = fracturing fluid viscosity (cp); H = fracture height (m); and t = time (s).

Also, the results were validated using another P3D model called the 3D tip-dominated model. This model is also found in the FracPro 2019 simulator. Extreme permeability contrast layers are considered by the 3D tip-dominated model. In this instance, the increase in fluid leak-off as the hydraulic fracture tip approaches a high permeability layer can stop the propagation of the fracture.

The parameters used in the model are shown in Table 5. The thickness of the shale formations was used as a constant height in KGD and PKN models. The rock in the formations are heterogeneous, hence they have different values of Young's modulus and Poison's ratios, and there is different in situ stress at different depths. Thus, the average values of these parameters were used in the KGD and PKN models.

Results and Discussion

Results

Fracturing Fluid Selection

In selecting the fracturing fluid, several fracturing fluid types were modeled in the simulator, and these fluids vary in viscosity and components. These fluids were mixed with the proppants of 20/40 mesh size. The simulation was conducted at a constant rate of 12.72 m^3/min. The results show that some linear gel fluids with HPG additives (Linear gel 30 and 40 GW-32) created wider and longer propped fractures compared to slickwater and water-based fluids (Table 6). Apart from the fractures created, linear gels have several advantages. Linear gel fluids contain gels that are capable of carrying high proppant concentrations. These fracturing fluids can control clay mineral swelling when mixed with KCl and reduce the tendency of a gas to form water drops due to the capillary forces, as explained by Parekh and Sharma (2004). The results of Mader (1989) showed that applying gel-loaded fluids brings better results in production. Also, Montgomery (2013) commented that linear gels have a low cost. Due to all these factors, linear gel fracturing fluids were suggested and used for further analysis.

After the suggestion of the fracturing fluid, different treatment parameters were analyzed, and their effects on the fracture propagation and geometries were evaluated. These factors include ten injection rates, six linear gel fracturing fluids, and three proppant sizes.

The Effects of Injection Rates

The effect of injection rates was analyzed by running simulations at different injection rates for various fracturing fluids, and the proppants used were of 20/40 mesh size. Generally, the results showed the increase in the injection rate led to an increase in fracture width and half-length (Figs. 6 and 7). At a low injection rate, the width was small, then the width increased at injection rates of 3.18 and 4.77 m^3/min when the injection rate reached 7.95 m^3/min the width dropped. The width increased again after an injection rate of 9.54 m^3/min. The fracturing fluid with gel loading of 30 ppgt (linear gel 30) created the widest fracture (1.27 cm) compared

Table 5. Parameters used in the validation of the simulator's results

Parameters	Units	Value
Fracture height	m	88.4
Average Young modulus	Pa	2.48×10^{10}
Average Poison's ratio	—	0.25
Fluid viscosity	cp	33
Pumping rate	m^3/min	6.3, 8, 12.72
Leak off coefficient	m/min^5	8.5333×10^{-6}
Passed time	min	0 to 100

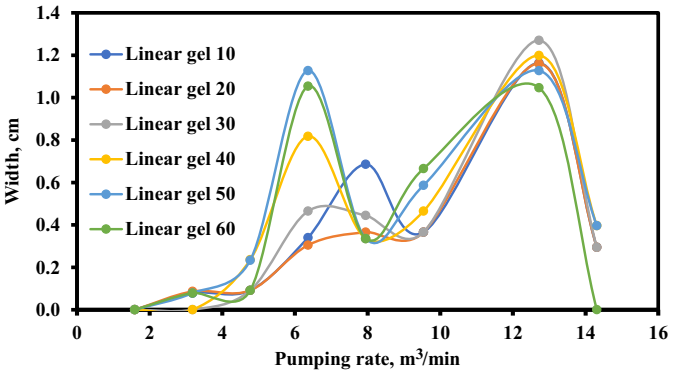

Fig. 6. Variation of fracture width at different injection rates for various fluids, maximum width was 1.27 cm at a pumping rate of 12.7 m^3/min, and the thinnest fracture at an injection rate of 12.7 m^3/min was 1.05 cm for fluid with gel loading of 60 ppgt.

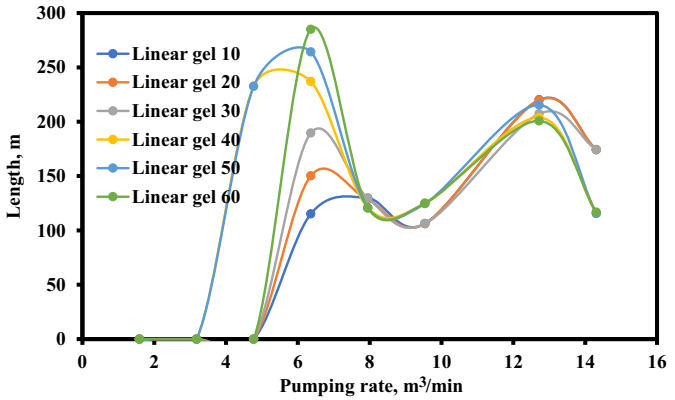

Fig. 7. Variation of fracture half-length at different injection rates for various fluids, the maximum length is 285 m at a pumping rate of 6.36 m^3/min.

Table 6. The fracture created by different kinds of fracturing fluids at a flow rate of 12.72 m^3/min (Proppants size 20/40 wire mesh size)

Serial number	Fluid type	Viscosity (cP)	Apparent viscosity (cP) at a shear rate of 511, at 82.2°C	Width (cm)	Propped height (m)	Propped half-length (m)
1	Slickwater	—	2.6	1.25	62.85	147.34
2	Linear gel 10 GW-32	—	2.1	1.16	69.01	166.21
3	Linear gel 20 GW-32	—	3.6	1.16	69.37	166.85
4	Linear gel 30 GW-32	—	8.1	1.27	91.47	207.32
5	Linear gel 40 GW-32	—	15.7	1.20	91.29	203.97
6	Linear gel 50 GW-32	—	23.9	1.13	67.30	158.95
7	Linear gel 60 GW-32	—	33	1.05	63.52	140.12
8	Water-based fluid	104	—	1.15	91.04	190.03
9	Water-based fluid with 65% CO_2	104	—	0.39	0	0
10	Water-based fluid with 65% N_2	104	—	0.39	0	0
11	Water-based fluid with 70% CO_2	104	—	0.85	89.98	169.19
12	Water-based fluid with 70% N_2	104	—	0.85	89.98	169.19
13	Water-based fluid with 75% N_2	104	—	0.39	0	0

to other fluids. This fluid developed the widest fracture at an injection rate of 12.72 m^3/min. Also, other fracturing fluids propagated the wider fractures at an injection rate of 12.72 m^3/min, except fluid with gel loading of 60 ppgt. Thus, at a pumping rate of 12.72 m^3/min, the thinnest fracture was 1.05 cm for fluid with gel loading of 60 ppgt. When the injection rate reached 14.31 m^3/min, the width dropped again (Fig. 6).

The fracture half-length developed by different fracturing fluids at different injection rates showed the same trend as the fracture width. The fracture half-length at lower injection rates was small, and then the length increased at the injection rate of 6.36 m^3/min. The fracture length dropped at the injection rate of 7.95 m^3/min. After the injection rate of 9.54 m^3/min, the fracture half-length increased again. The maximum fracture half-length was obtained at an injection rate of 6.36 m^3/min by the fluids with gel loading of 60 ppgt; that length was 285.05 m. At a pumping rate of 6.36 m^3/min, the fluid gel loading of 10 ppgt created the shortest fracture (115.18 m) compared to all other fluids (Fig. 7).

Effects of Gel Loading (Polymer Concentration)

The created fracture width and half-length at different gel loading can be used to examine the impact of polymer concentration, as depicted in Figs. 6 and 7. The increase in gel loading implies an increase in the fluid viscosity, as shown in Table 6, and more gel-loading fluid has high apparent viscosity. In the highly viscous fluid (60 ppgt), the fracture half-length developed at an injection rate of 6.36 m^3/min was the highest compared to all half-lengths created by other fluids. Other fracturing fluids which show higher fracture half-length are fluids with gel loading of 40 and 50 ppgt at an injection rate of 6.36 m^3/min. A fracturing fluid with a gel loading of 10 ppgt developed the smallest fracture half-length, followed by a fracturing fluid with a gel loading of 20 ppgt (Fig. 7).

The variation of fracture width with the polymer concentration is shown in Fig. 6. The fluid developed the widest fracture with gel loading of 30 ppgt at an injection rate of 12.72 m^3/min. On the other hand, other fluids which developed wider fractures were fluids with gel loading of 40 and 50 ppgt at an injection rate of 12.72 m^3/min. In contrast, fluid with gel loading of 60 ppgt developed the thinnest fracture compared to other fluids. Also, the thinner fracture was created by fluid with gel loading of 30 ppgt and 50 ppgt.

Influence of Proppant Size

The effect of proppants was analyzed for different fracturing fluids at an injection rate of 6.36 m^3/min since this injection rate propagated the most extended fractures for most fracturing fluids compared to other injection rates. Three sizes of proppant were run in the model, and those proppants include 12/20, 20/40, and 40/70 mesh sizes.

Table 7 shows the simulated results of the propped half-length for different proppant sizes. The proppant with a 12/20 mesh size developed the longest propped half-length compared to other proppants sizes. The largest propped half-length was archived by fluid with a gel loading of 60 ppgt. Thus, this implies that high-viscous fluid can transport large-sized proppants deep in the fracture. Also, large-sized proppants develop higher permeability when compared to small-sized proppants, as shown in Table 4.

Table 7. Propped fracture half-length (m) developed by proppant with 20/40, 12/20, and 40/70 mesh sizes at an injection rate of 6.36 m^3/min

Gel loading (ppgt)	Proppants sizes		
	20/40	12/20	40/70
Slick water	0	0	0
10	0	115.7021	0
20	0	0	0
30	0	0	0
40	113.2637	174.7418	255.6967
50	264.2921	235.8847	167.3962
60	234.3607	264.8407	210.8606

Combining the Effects of Injection Rate, Fluid Type and Proppant Size

The effects of both fluid types, injection rates and proppants sizes were analyzed as shown in Figs. 8 and 9. This analysis was conducted for three fluid types, which are fluids with gel loading of 40, 50 and 60 ppgt. These were the fluids that developed longer fractures when compared to other fluids. The results show that the fracturing fluid with gel loading 50 ppgt when mixed with proppants of 12/20 mesh-size at the injected rate of 12.72 m^3/min developed the widest fracture (1.84 cm) when compared to all other scenarios. Other scenarios which show better results are fracturing fluid with

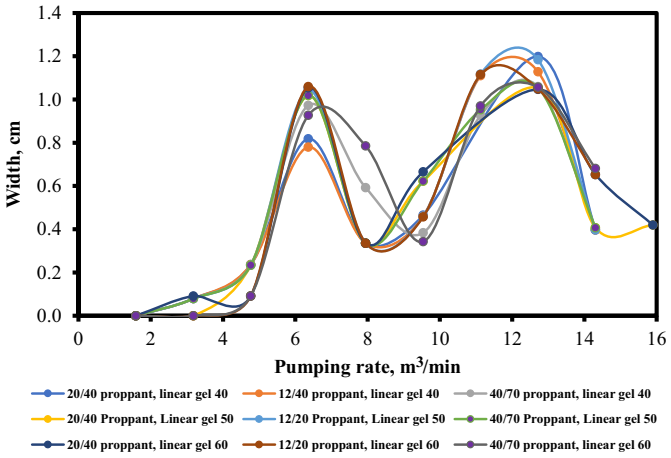

Fig. 8. Fracture widths at various injection rates for a fracturing fluid with different polymer concentrations and containing different proppants sizes, maximum width is 1.18 cm at an injection rate of 12.72 m^3/min.

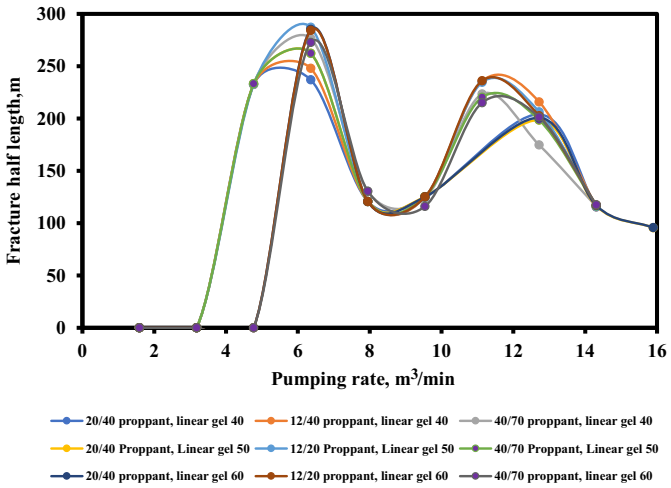

Fig. 9. Fracture half-lengths at various injection rates for a fracturing fluid with different polymer concentrations and containing different proppants sizes; the maximum length is 287.12 m at a pumping rate of 6.36 m^3/min.

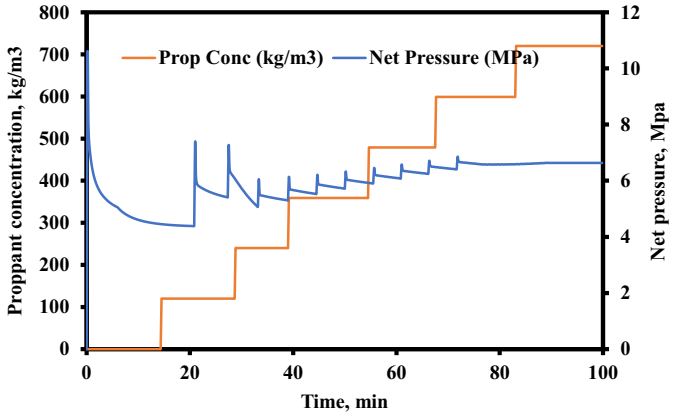

Fig. 10. Variation of net pressure, proppant concentration and slurry rate during the fracturing time.

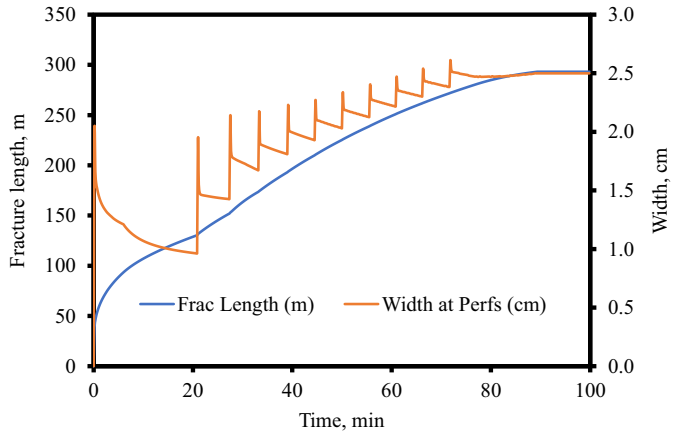

Fig. 11. Development of fracture length and width during the fracturing time.

gel loading of 40 ppgt mixed with proppants with 12/20 mesh size at an injection rate of 12.72 m^3/min. They were also fracturing fluid with gel loading of 60 ppgt mixed with proppants with 12/20 mesh size at an injection rate of 11.13 m^3/min and fracturing fluid with gel loading of 60 ppgt mixed with proppants with 40/70 mesh size at an injection rate of 12.72 m^3/min (Fig. 8).

Fig. 9 shows the results of the fracture half-length obtained from different scenarios. The results showed maximum fracture half-length (287.12 m) was developed by fluid with gel loading of 50 ppgt when mixed with proppants with 12/20 mesh size at an injection rate of 6.36 m^3/min. On the other hand, the fracturing fluids with gel loading 60 ppgt mixed with proppants of 12/20 mesh size at an injection rate of 6.36 m^3/min showed better results, whereby fracture developed was having half-length of 284.26 m. But the propped half-length for fluid with gel loading of 60 ppgt, when mixed with proppants of 12/40 mesh size, was larger when compared to propped half-length developed by fluid with gel loading of 50 ppgt when mixed with proppants of 12/20 mesh size (Table 7).

Discussion

The performance of different fracturing fluids shows that fluid with gel loading of 50 and 60 ppgt developed longer and wider fractures compared to other fluids. But a fluid with gel loading of 60 ppgt developed the longest propped fracture. Therefore, this fluid was chosen as a fracturing fluid in these shales' formations. This fluid has an apparent viscosity of 33 cp, which is the highest compared to other linear gel fracturing fluids. Fluid with gel loading of 60 ppgt developed the longest propped fracture since it can carry and transport a large concentration of proppants and create a wider fracture. These results agreed with other scholars like Montgomery (2013), who found that high-viscous fluid can develop wider fractures enough for proppants to pass, generating a desired net pressure to control height growth and fluid loss. According to Bokane et al. (2013), the fluid viscosity shows better proppants distribution when the injection rate is low, and proppants of small density are used. Also, Saberhosseini et al. (2017) conducted a study and found that

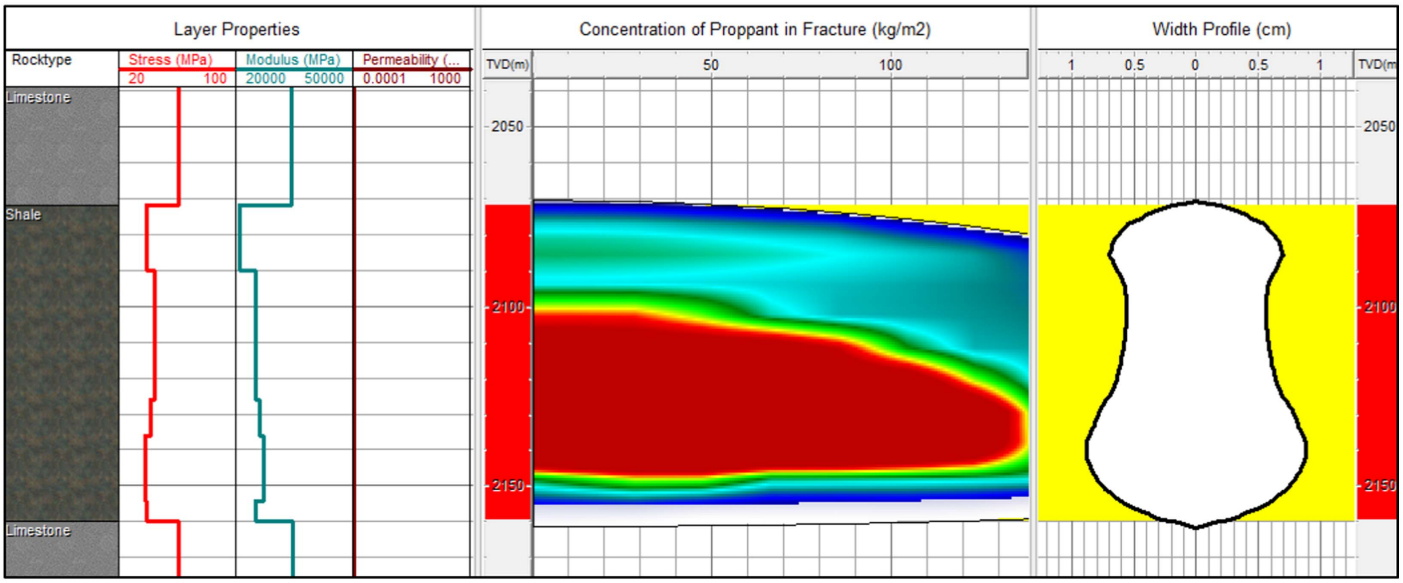

Fig. 12. Predicted fracture with propped fracture half of 264.8 m and an average width of 1.06 cm.

an increase in fluid viscosity from 10^{-3} to 10 Pa.s caused an increase in fracture width from 8.83 to 13.3 mm.

Among the three proppant sizes modeled in this study, the 12/20 mesh size proppant is the one that was able to be propped at a deeper length when compared to other sizes. Proppants with 12/20 mesh size have a larger size when compared to other types of proppant used. The high viscosity of fracturing fluid helped in carrying and transporting these large proppants to the deep of the fracture. Also, large-sized proppants develop higher conductivity in the formation when compared to small-sized proppants. For these reasons, the proppants with 12/20 were suggested to be used in these formations.

The effect of injection rate was analyzed by running the model at the injection rate from 1.59 to 15.90 m^3/min. The longer fractures were developed at an injection rate of 6.36 m^3/min, whereas the wider fracture was developed at an injection rate of 12.72 m^3/min. The injection rate of 6.36 m^3/min was selected since it created a longer fracture. Longer fracture increases more contact area with the reservoir compared to the wider fracture (Since the width is very small compared to the length). Thus, it is suggested to use the pump capable of developing this injection rate. The study conducted by Morgan et al. (2017) shows that an increase in injection rate causes an increase in the breakdown pressure. Also, Solberg et al. (1980) observed a log-linear relationship between injection rate and breakdown pressure. Therefore, an increase in injection rate causes an increase in the breakdown pressure, which increase fracture half-length and width. But this work shows the best operating injection rate was 6.36 m^3/min. The fracture half-length decreased when the injection rate was higher than 6.36 m^3/min, and this could be due development of fluid leak-off. Therefore, increasing the injection rate causes the rise of fracturing pressure. According to Shen and Zhang (2019), casing deformation can occur when there is high fracturing pressure. Deformation of the casing can cause fluid leak-off, reducing the fracturing fluid's ability to extend the fracture (Figs. 13 and 14).

The Influence of Hydraulic Fracture Treatment Parameters Suggested on the Fracture Development

The fluid with gel loading of 60 ppgt and proppant with 12/20 mesh size was suggested to be used in the Longmaxi and Wufeng shale formations. The slurry fluid was injected into the formations at the constant rate of 6.36 m^3/min. When the slurry fluid was pumped into the formation, the proppants concentration increased with time, as shown in Fig. 10. Also, the injection of slurry fluid into the formation caused the rise of net pressure. In the beginning, the net pressure was highly increased, and then the net pressure slightly varied with time, as shown in Fig. 10.

Generally, the results show that both fracture length and width increased with time. However, in the initial 18 minutes, the fracture width grew, then decreased again (Fig. 11). Additionally, the trend of rising net pressure appears to be followed by the expansion of fracture width (Figs. 10 and 11). The final results of the fracture geometry developed during the hydraulic fracturing process are shown in Fig. 12. The fracture with propped half-length of 264.8 m and an average width of 1.06 cm was formed. Also, Fig. 12 indicates that the stress contrast in the shale formations affected the shape of the fracture, the interval with higher stress were having smaller width when compared to the interval with low stress. These dimensions provide enough surface area for the reservoir fluid to flow from the reservoir to the production well and facilitate the required production rate.

Validation of the Results

The results show that the fracture geometry developed by the 3D shear decoupled model is very close to the fracture developed by another simulator model, the 3D tip-dominated model. The fracture length from the 3D shear decoupled model is a bit far from the fracture length from the PKN model, and still, it differs a lot from the KGD model, as shown in Fig. 13. But also, the fracture width developed by two simulator models, the 3D shear decoupled and the 3D tip-dominated models are very close. Also, the PKN model shows better closeness with simulator results in developing the width (Fig. 14). All these results show a significant difference between the KGD model and simulator models (3D shear decoupled

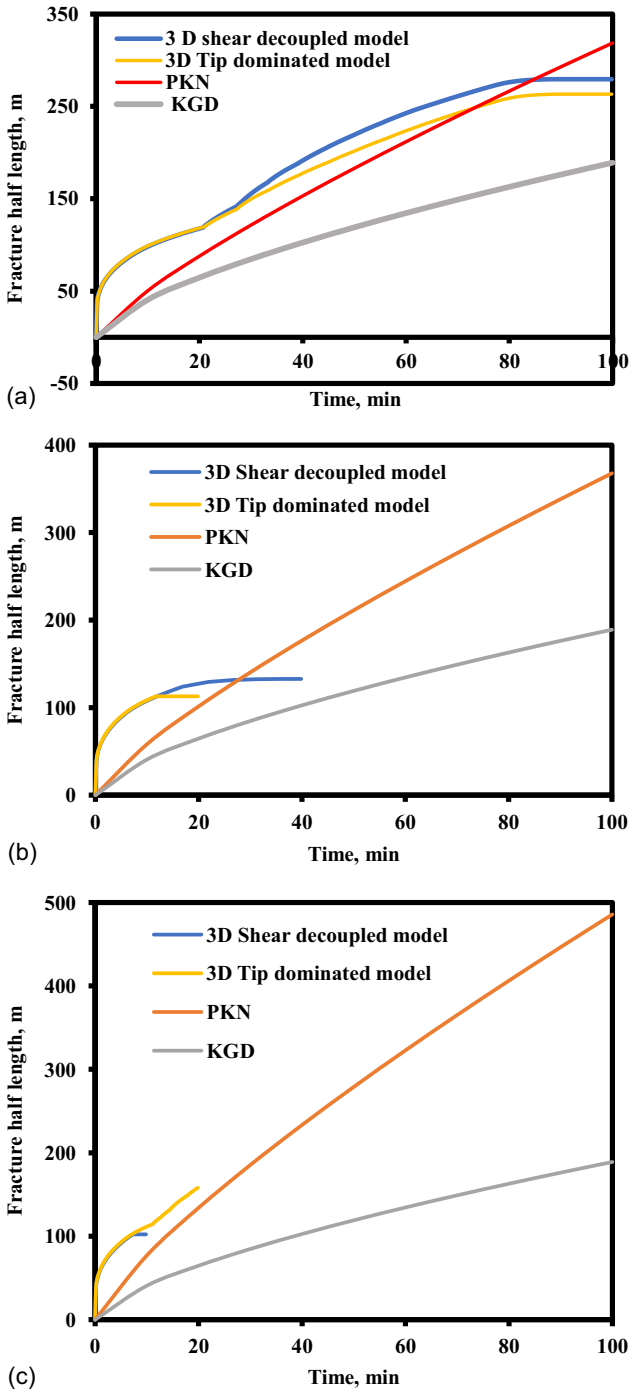

Fig. 13. Fracture half-length developed after applying the 3D shear decoupled model (Simulator), KGD model, PKN model, and 3D tip-dominated model (simulator) at different injection rates: (a) injection rate 6 m^3/min; (b) injection rate 8 m^3/min; and (c) injection rate 12.72 m^3/min.

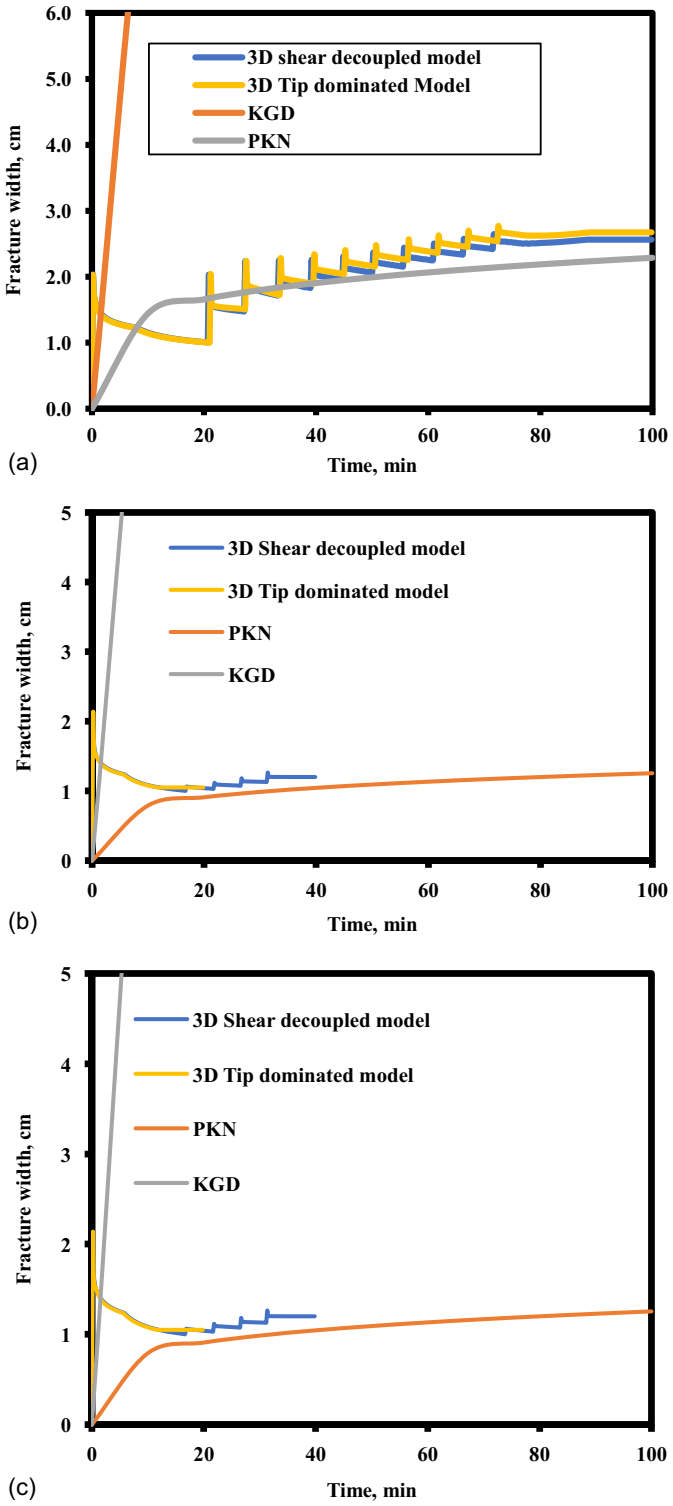

Fig. 14. Fracture width developed after applying the 3D shear decoupled model (Simulator), KGD model, PKN model, and 3D tip-dominated model (simulator) at different injection rates: (a) injection rate 6 m^3/min; (b) injection rate 8 m^3/min; and (c) injection rate 12.72 m^3/min.

model and 3D tip-dominated model). But also, there is a slight difference between the PKN model results and the simulator results. A small difference in those results indicated that the results from the simulator could be used in the prediction of fracture geometry. The slight difference in the results between the PKN model

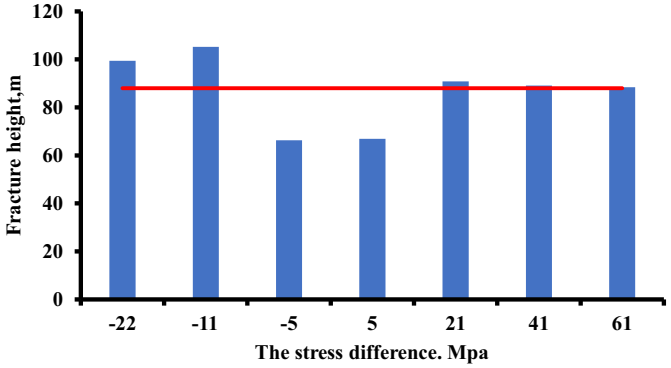

Fig. 15. Fracture heights developed as a result of the stress difference between the Shale formation and layers above and below the shale formation. Negative values on the x-axis indicates lower stresses in the layers above and below the shale formation, and positive values on the x-axis indicate higher stresses. The red line indicates the thickness of the shale formation.

and the simulator models is caused by several factors. Using the average value of the input parameters instead of the values recorded at each depth used in the simulator is one of the factors which causes the difference in results. Also, reservoir conditions such as temperature, permeability, and leak-off coefficient are not included in the PKN model, causing deviation in the results. The results show that initially, the leak-off was not significant, but later it became substantial, leading to a shorter length in 3D models than was determined by the PKN model. The findings are corroborated by (Nordgren 1972), who demonstrated how fluid leak-off might become significant after a specific amount of time and introduced the concept of dimensionless time to determine when the leak-off will be significant. Additionally, compared to low injection rates, greater injection rates caused a higher leak-off (Yang et al. 2016). The higher fluid leak-off led to a shorter fracture length, as illustrated in Fig. 13.

The Impact of Stress Contrast on the Geometry of the Fracture

The stress in the layer above and below the shale formations was assumed to be 60 MPa in the aforementioned situations because it was not present. Therefore, stress contrasts were analyzed to determine the impact of stress contrast between shale formations and the strata above and below. The results show that the fracture grew in the shale formations when the stress in the layer above and below was higher than in the shale formations (positive value in Fig. 15). Therefore, the higher stress in the layer above and below the shale formations acted as a stress barrier. But when the layers above and below the shale formations had much lower stress, the fracture prolonged in the layers above and below the shale formations. In this case, wider and short fractures were formed (Table 8). But the layers above and below the shale formations were limestone layers. According to Huo et al. (2021), limestone lithologies have greater Young's modulus, compressive strength, and in situ stress than shale lithology. Thus, the fracturing pressure for limestone lithology is higher than that of shale lithology. Furthermore, the study discovered that shale formations are easier to fracture than limestone lithologies. Therefore, when the shale formation is sandwiched between underlying and overlying limestone lithology, the fracture will be contained in the shale formation. This scenario is seen where stress contrasts were higher (greater stress in the layer above and below the shale formation).

Table 8. The impact of stress contrast between the shale formation and the layer above and below

Stress difference (MPa)	Stress	Length (m)	Width (cm)	Height (m)	Comments
+5	44	106	0.348	66.9	—
+21	60	284.3	1.06	90.8	—
+41	80	281	1.091	89.1	—
+61	100	293.1	1.055	88.4	—
−5	34	111.7	1.033	66.3	—
−11	28	182.2	1.547	105.2	Fractures develop outside the shale formations
−21	17	260.5	1.159	99.4	Fracture develops outside the shale formations

Conclusion

Lower Silurian Longmaxi and Upper Ordovician Wufeng shale formations are normally pressured formations found in the Chongqing region, southeast of the Sichuan Basin in southwestern China. Both are tight shale formations that require hydraulic fracturing to produce shale gas commercially. Therefore, hydraulic fracturing simulation was conducted to study the influence of different parameters on the development of hydraulic fracture in these formations. The following conclusions are reached from this work and suggested for the optimal stimulation of these shale gas formations.

1. The developed fracture length and width increase with increasing volumetric injection rate. The increase in volumetric injection rate causes the increase of the breakdown pressure in the fracture as a result of increasing the fracture size.
2. The developed fracture width and propped fracture length increase with increasing gel loading. Thus, this is because the gel loading seals the micro-cracks in this tectonically complex shale formation. This sealing reduces the leak-off in the under-to-normally pressured shale reservoir, hence increasing the breakdown pressure, which increases the width. Also, high-viscous fluid can carry the proppants deep in the fracture.
3. The highest gel loading fluid (60 ppgt), when mixed with proppants of 12/20 mesh size and injected at a rate of 6.36 m^3/min, created the longest propped fracture length compared to other scenarios. The application of these parameters in these formations developed a fracture with an average width of 1.06 cm and propped half-length of 264.8 m.
4. The formations' stress contrast affects the shape of the fracture, the interval with lower stress had large widths when compared to the interval with high stress. Also, the higher stress in the layers above and below the shale formations contains the fracture height and hence favors the growth of fracture in the shale formations.

Data Availability Statement

All data, models, and code generated or used during the study appear in the published article.

Acknowledgments

The authors would like to acknowledge the financial support of the National Natural Science Foundation of China (No. 42130803). Also, special thanks are given to the China Scholarship Council (CSC No. 2019GBJ002427) for sponsoring the first author to study and conduct research at the China University of Geosciences at Wuhan.

References

Abaa, K., J. Y. Wang, and M. T. Ityokumbul. 2012. "Parametric study of fracture treatment parameters for ultratight gas reservoirs." In *Proc., SPE Americas Unconventional Resources Conf.* Richardson, TX: OnePetro. https://doi.org/10.2118/152877-MS.

Adachi, J., E. M. Siebrits, A. Peirce, and J. Desroches. 2007. "Computer simulation of hydraulic fractures." *Int. J. Rock Mech. Min. Sci.* 44 (5): 739–757. https://doi.org/10.1016/j.ijrmms.2006.11.006.

Adachi, J. I., E. Detournay, and A. P. Peirce. 2010. "Analysis of the classical pseudo-3D model for hydraulic fracture with equilibrium height growth across stress barriers." *Int. J. Rock Mech. Min. Sci.* 47 (4): 625–639. https://doi.org/10.1016/j.ijrmms.2010.03.008.

Ahmed, S., A. S. Hanamertani, and M. R. Hashmet. 2019. "CO 2 foam as an improved fracturing fluid system for unconventional reservoir." In *Exploitation of unconventional oil and gas resources-hydraulic fracturing and other recovery and assessment techniques*. London: IntechOpen.

Al-Sadhan, N. 2014. *Prediction of short-term and long-term baseline conductivity degradation for proppants of different types and sizes*. Golden, CO: Colorado School of Mines.

Aminzadeh, F. 2018. "Hydraulic fracturing: An overview." *J. Sustainable Energy Eng.* 6 (3): 204–228. https://doi.org/10.7569/JSEE.2018.629512.

Annigeri, B. S., and M. P. Cleary. 1984. "Surface integral finite element hybrid (SIFEH) method for fracture mechanics." *Int. J. Numer. Methods Eng.* 20 (5): 869–885. https://doi.org/10.1002/nme.1620200507.

Azad, M., M. Ghaedi, A. Farasat, H. Parvizi, and H. Aghaei. 2022. "Case study of hydraulic fracturing in an offshore carbonate oil reservoir." *Pet. Res.* 7 (4): 419–429. https://doi.org/10.1016/j.ptlrs.2021.12.009.

Barati, R., and J. T. Liang. 2014. "A review of fracturing fluid systems used for hydraulic fracturing of oil and gas wells." *J. Appl. Polym. Sci.* 131 (16): 15. https://doi.org/10.1002/app.40735.

Belyadi, H., E. Fathi, and F. Belyadi. 2019. *Hydraulic fracturing in unconventional reservoirs: Theories, operations, and economic analysis*. Oxford, UK: Gulf Professional Publishing.

Bokane, A., S. Jain, Y. Deshpande, and F. Crespo. 2013. "Transport and distribution of proppant in multistage fractured horizontal wells: A CFD simulation approach." In *Proc., SPE Annual Technical Conf. and Exhibition*. Richardson, TX: OnePetro. https://doi.org/10.2118/166096-MS.

Cao, X., M. Wang, J. Kang, S. Wang, and Y. Liang. 2020. "Fracturing technologies of deep shale gas horizontal wells in the Weirong Block, southern Sichuan Basin." *Nat. Gas Ind. B* 7 (1): 64–70. https://doi.org/10.1016/j.ngib.2019.07.003.

Chamanzad, M., A. Ramezanzadeh, B. Tokhmechi, and H. Norouzi. 2017. "Comparison of different hydraulic fracture growth models based on a carbonate reservoir in Iran." *J. Chem. Pet. Eng.* 51 (2): 95–104. https://doi.org/10.22059/jchpe.2017.232270.1191.

Chen, F., S. Lu, X. Ding, and X. He. 2018. "Shale gas reservoir characterization: A typical case in the southeast Chongqing of Sichuan Basin, China." *PLoS One* 13 (6): E0199283. https://doi.org/10.1371/journal.pone.0199283.

Chen, X., J. Zhao, Y. Li, W. Yan, and X. Zhang. 2019. "Numerical simulation of simultaneous hydraulic fracture growth within a rock layer: Implications for stimulation of low-permeability reservoirs."

J. Geophys. Res. Solid Earth 124 (12): 13227–13249. https://doi.org/10.1029/2019JB017942.

Cholet, H. 2008. *Well production practical handbook*. Paris: Editions Technip.

Cipolla, C. L., and C. A. Wright. 2000. "Diagnostic techniques to understand hydraulic fracturing: What? why? and how?" In *Proc., SPE/CERI Gas Technology Symp*. Richardson, TX: OnePetro.

Cui, G., W. Wang, B. Dou, Y. Liu, H. Tian, J. Zheng, and Y. Liu. 2022. "Geothermal energy exploitation and power generation via a single vertical well combined with hydraulic fracturing." *J. Energy Eng.* 148 (1): 04021058. https://doi.org/10.1061/(ASCE)EY.1943-7897.0000809.

Da, Q.-A., C.-J. Yao, X. Zhang, X.-P. Wang, X.-H. Qu, and G.-L. Lei. 2022. "Investigation on microscopic invasion characteristics and retention mechanism of fracturing fluid in fractured porous media." *Pet. Sci.* 19 (4): 1745–1756. https://doi.org/10.1016/j.petsci.2022.03.009.

Dai, J., Y. Ni, D. Gong, Z. Feng, D. Liu, W. Peng, and W. Han. 2017. "Geochemical characteristics of gases from the largest tight sand gas field (Sulige) and shale gas field (Fuling) in China." *Mar. Pet. Geol.* 79 (Jan): 426–438. https://doi.org/10.1016/j.marpetgeo.2016.10.021.

Dong, D., Y. Wang, X. Li, C. Zou, Q. Guan, C. Zhang, and H. Liu. 2016. "Breakthrough and prospect of shale gas exploration and development in China." *Nat. Gas Ind. B* 3 (1): 12–26. https://doi.org/10.1016/j.ngib.2016.02.002.

Duan, H., H. Li, J. Dai, and Y. Wang. 2019. "Horizontal well fracturing mode of 'increasing net pressure, promoting network fracture and keeping conductivity' for the stimulation of deep shale gas reservoirs: A case study of the Dingshan area in SE Sichuan Basin." *Nat. Gas Ind. B* 6 (5): 497–501. https://doi.org/10.1016/j.ngib.2019.02.005.

Economides, M. J., and K. G. Nolte. 1989. *Reservoir stimulation*. New York: Prentice Hall Englewood Cliffs.

Esfandiari, M., and A. Pak. 2022. "XFEM modeling of the effect of in-situ stresses on hydraulic fracture characteristics and comparison with KGD and PKN models." *J. Pet. Explor. Prod. Technol.* 2022 (Jul): 1–17. https://doi.org/10.1007/s13202-022-01545-7.

Geertsma, J., and R. Haafkens. 1979. "A comparison of the theories for predicting width and extent of vertical hydraulically induced fractures." *J. Energy Resour. Technol.* 101 (1): 8–19. https://doi.org/10.1115/1.3446866.

Ghahremani, N., and L. Clapp. 2014. "Feasibility of using brackish groundwater desalination concentrate as hydraulic fracturing fluid in the Eagle Ford Shale." In *Shale energy engineering 2014: Technical challenges, environmental issues, and public policy*, 23–32. Reston, VA: ASCE.

Gidley, J. L. 1989. *Recent advances in hydraulic, monograph*. Richardson, TX: Society of Petroleum Engineers.

Guo, B., W. C. Lyons, and A. Ghalambor. 2007. "Petroleum production engineering." In *Hydraulic fracturing*. Burlington, NJ: Gulf Professional Publishing.

Guo, C., J. Sun, and H. Liu. 2021. "Transport model for gas and water in nanopores of shale gas reservoirs." *J. Energy Eng.* 147 (4): 04021022. https://doi.org/10.1061/(ASCE)EY.1943-7897.0000771.

Guo, T.-K., Z.-L. Luo, J. Zhou, Y.-Z. Gong, C.-L. Dai, J. Tang, and J.-J. Ge. 2022. "Numerical simulation on proppant migration and placement within the rough and complex fractures." *Pet. Sci.* 19 (5): 2268–2283. https://doi.org/10.1016/j.petsci.2022.04.010.

Haddad, M., A. Sanaei, and K. Sepehrnoori. 2017. "Hydraulic fracturing fluid effect on clay swelling in stimulated naturally fractured reservoirs." In *Proc., SPE/AAPG/SEG Unconventional Resources Technology Conf.* Houston: Society of Exploration Geophysicists.

Huang, H., T. Babadagli, H. A. Li, K. Develi, and G. Wei. 2019. "Effect of injection parameters on proppant transport in rough vertical fractures: An experimental analysis on visual models." *J. Pet. Sci. Eng.* 180 (1): 380–395. https://doi.org/10.1016/j.petrol.2019.05.009.

Huo, Z., J. Gao, J. Zhang, D. Zhang, and Y. Liang. 2021. "Role of overlying and underlying limestones in the natural hydraulic fracturing of shale sections: The case of marine–continental transitional facies in the Southern North China Basin." *Energy Rep.* 7 (65): 8711–8729. https://doi.org/10.1016/j.egyr.2021.11.025.

Jiang, S., Y. Peng, B. Gao, J. Zhang, D. Cai, G. Xue, and N. Dahdah. 2016a. "Geology and shale gas resource potentials in the Sichuan Basin, China." *Energy Explor. Exploit.* 34 (5): 689–710. https://doi.org/10.1177/0144598716657442.

Jiang, S., Z. Xu, Y. Feng, J. Zhang, D. Cai, L. Chen, and S. Long. 2016b. "Geologic characteristics of hydrocarbon-bearing marine, transitional and lacustrine shales in China." *J. Asian Earth Sci.* 115 (Jan): 404–418. https://doi.org/10.1016/j.jseaes.2015.10.016.

Korsch, R., M. Huazhao, S. Zhaocai, and J. Gorter. 1991. "The Sichuan basin, southwest China: A late proterozoic (Sinian) petroleum province." *Precambrian Res.* 54 (1): 45–63. https://doi.org/10.1016/0301-9268(91)90068-L.

Li, S., J. Yang, B. Jiang, Q. Jiang, X. Wei, and L. Yang. 2022. "Analysis of physical properties and influencing factors of Longmaxi Shale in Sichuan Basin." *J. Energy Eng.* 148 (6): 04022034. https://doi.org/10.1061/(ASCE)EY.1943-7897.0000856.

Liang, F., M. Sayed, G. A. Al-Muntasheri, F. F. Chang, and L. Li. 2016. "A comprehensive review on proppant technologies." *Petroleum* 2 (1): 26–39. https://doi.org/10.1016/j.petlm.2015.11.001.

Liu, R., D. Jiang, J. Zheng, F. Hao, C. Jing, H. Liu, and G. Wei. 2021. "Stress heterogeneity in the Changning shale-gas field, southern Sichuan Basin: Implications for a hydraulic fracturing strategy." *Mar. Pet. Geol.* 132 (6): 105218. https://doi.org/10.1016/j.marpetgeo.2021.105218.

Liu, S., L. Zhang, Z. Wang, and Z. Dong. 2022. "Analysis of the influence of dual spark plugs on the combustion stability of a shale-gas engine." *J. Energy Eng.* 148 (1): 04021064. https://doi.org/10.1061/(ASCE)EY.1943-7897.0000817.

Liu, Y., N. Qiu, Q. Yao, and C. Zhu. 2017. "The impact of temperature on overpressure unloading in the central Sichuan Basin, southwest China." *J. Pet. Sci. Eng.* 156 (Jul): 142–151. https://doi.org/10.1016/j.petrol.2017.05.010.

Long, G., and G. Xu. 2017. "The effects of perforation erosion on practical hydraulic-fracturing applications." *SPE J.* 22 (2): 645–659. https://doi.org/10.2118/185173-PA.

Luo, Z. L. 1998. "New recognition of basement in Sichuan Basin." *J. Chengdu Univ. Tech.* 25 (2): 191–200.

Lutynski, M. A. 2015. "A method of proppant pack permeability assessment." *Phys. Probl. Mineral Process.* 2015 (1): 51. https://doi.org/10.5277/ppmp150129.

Mader, D. 1989. *Hydraulic proppant fracturing and gravel packing*. New York: Elsevier.

Mgimba, M. M., S. Jiang, and G. C. Mwakipunda. 2022. "The identification of normal to underpressured formations in the Southeastern Sichuan basin." *J. Pet. Sci. Eng.* 219 (Dec): 111085. https://doi.org/10.1016/j.petrol.2022.111085.

Montgomery, C. 2013. "Fracturing fluids." In *Proc., ISRM Int. Conf. for Effective and Sustainable Hydraulic Fracturing*. Brisbane, Australia: Society of Petroleum Engineers.

Morgan, S. P., B. Q. Li, and H. H. Einstein. 2017. "Effect of injection rate on hydraulic fracturing of Opalinus clay shale." In *Proc., 51st US Rock Mechanics/Geomechanics Symp*. San Francisco: Society of Petroleum Engineers.

Muther, T., M. J. Khan, M. H. Chachar, and H. Aziz. 2020. "A Study on designing appropriate hydraulic fracturing treatment with proper material selection and optimized fracture half-length in tight multilayered formation sequence." *SN Appl. Sci.* 2 (5): 1–12. https://doi.org/10.1007/s42452-020-2729-9.

Nguyen, H. T., J. H. Lee, and K. A. Elraies. 2020. "A review of PKN-type modeling of hydraulic fractures." *J. Pet. Sci. Eng.* 195 (10): 107607. https://doi.org/10.1016/j.petrol.2020.107607.

Nguyen, H. T., J. H. Lee, and K. A. Elraies. 2022. "Review of pseudo-three-dimensional modeling approaches in hydraulic fracturing." *J. Pet. Explor. Prod. Technol.* 12 (4): 1095–1107. https://doi.org/10.1007/s13202-021-01373-1.

Nie, H., Z. Jin, X. Ma, Z. Liu, T. Lin, and Z. Yang. 2017. "Dispositional characteristics of Ordovician Wufeng formation and Silurian Longmaxi formation in Sichuan Basin and its adjacent areas." *Pet. Res.* 2 (3): 233–246. https://doi.org/10.1016/j.ptlrs.2017.01.003.

Nordgren, R. 1972. "Propagation of a vertical hydraulic fracture." *Soc. Pet. Eng. J.* 12 (4): 306–314. https://doi.org/10.2118/3009-PA.

Olmen, B. D., D. A. Anschutz, H. D. Brannon, and K. M. Stribling. 2018. "Evolving proppant supply and demand: The implications on the hydraulic fracturing industry." In *Proc., SPE Annual Technical Conf. and Exhibition*. Richardson, TX: OnePetro. https://doi.org/10.2118/191591-MS.

Palmer, I. D., and H. R. Craig. 1984. "Modeling of asymmetric vertical growth in elongated hydraulic fractures and application to first MWX stimulation." In *Proc., SPE Unconventional Gas Recovery Symp*. Richardson, TX: OnePetro. https://doi.org/10.2118/12879-MS.

Parekh, B., and M. M. Sharma. 2004. "Cleanup of water blocks in depleted low-permeability reservoirs." In *Proc., SPE Annual Technical Conf. and Exhibition*. Richardson, TX: OnePetro. https://doi.org/10.2118/89837-MS.

Rahman, M., and M. Rahman. 2010. "A review of hydraulic fracture models and development of an improved pseudo-3D model for stimulating tight oil/gas sand." *Energy Sources Part A* 32 (15): 1416–1436. https://doi.org/10.1080/15567030903060523.

Saberhosseini, S. E., R. Keshavarzi, and K. Ahangari. 2017. "A fully coupled three-dimensional hydraulic fracture model to investigate the impact of formation rock mechanical properties and operational parameters on hydraulic fracture opening using cohesive elements method." *Arabian J. Geosci.* 10 (7): 1–8. https://doi.org/10.1007/s12517-017-2939-7.

Sadrpanah, H., T. Charles, and J. Fulton. 2006. "Explicit simulation of multiple hydraulic fractures in horizontal wells." In *Proc., SPE Europec/EAGE Annual Conf. and Exhibition*. Richardson, TX: OnePetro. https://doi.org/10.2118/99575-MS.

Settari, A., and M. P. Cleary. 1986. "Development and testing of a pseudo-three-dimensional model of hydraulic fracture geometry." *SPE Prod. Eng.* 1 (6): 449–466. https://doi.org/10.2118/10505-PA.

Shel, E. V., and G. V. Paderin. 2019. "Analytical solution of the pseudo-3D model for hydraulic fracturing in a storage-dominated regime." *Int. J. Rock Mech. Min. Sci.* 114 (5): 92–100. https://doi.org/10.1016/j.ijrmms.2018.12.020.

Shen, X., and P. Zhang. 2019. "A calculation method for the allowable fracturing injection pressure of preventing casing deformation." *Nat. Gas Ind. B* 6 (4): 384–393. https://doi.org/10.1016/j.ngib.2019.01.014.

Siddhamshetty, P., S. Mao, K. Wu, and J. S.-I. Kwon. 2020. "Multi-size proppant pumping schedule of hydraulic fracturing: Application to a MP-PIC model of unconventional reservoir for enhanced gas production." *Processes* 8 (5): 570. https://doi.org/10.3390/pr8050570.

Society of Petroleum Engineers. 2012. "Acid fracturing." Accessed October 10, 2012. http://petrowiki.org/Acid_fracturing.

Solberg, P., D. Lockner, and J. D. Byerlee. 1980. "Hydraulic fracturing in granite under geothermal conditions." *Proc., Int. J. Rock Mech. Min. Sci. Geomech. Abstr.* 17 (1): 25–33. https://doi.org/10.3390/pr8050570.

Soliman, M., J. L. Hunt, and A. El Rabaa. 1990. "Fracturing aspects of horizontal wells." *J. Pet. Technol.* 42 (8): 966–973. https://doi.org/10.2118/18542-PA.

Wang, J., X. Tan, J. Wang, H. Zhang, Y. Zhang, D. Guo, X. Wang, Z. Lei, C. Zeng, and G. Yao. 2021a. "Characteristics and genetic mechanisms of normal-pressure fractured shale reservoirs: A case study from the Wufeng–Longmaxi formation in southeastern Chongqing, China." *Front. Earth Sci.* 9 (2): 258. https://doi.org/10.3389/feart.2021.661706.

Wang, P., C. Zhang, A. Liu, P. Zhang, Y. Qiu, X. Li, S. Yu, S. Yao, S. Liu, and Z. Jiang. 2021b. "Slope belts of paleouplifts control the pore structure of organic matter of marine shale: A comparative study of lower Cambrian rocks in the Sichuan basin." *Geofluids* 2021 (Jun): 5517655. https://doi.org/10.1155/2021/5517655.

Wang, W., C. Lin, X. Zhang, C. Dong, L. Ren, and J. Lin. 2020. "Effect of burial history on diagenetic and reservoir-forming process of the Oligocene sandstone in Xihu sag, East China Sea Basin." *Mar. Pet. Geol.* 112 (Feb): 104034. https://doi.org/10.1016/j.marpetgeo.2019.104034.

Wangen, M. 2011. "Finite element modeling of hydraulic fracturing on a reservoir scale in 2D." *J. Pet. Sci. Eng.* 77 (3–4): 274–285. https://doi.org/10.1016/j.petrol.2011.04.001.

Wangen, M. 2013. "Finite element modeling of hydraulic fracturing in 3D." *Comput. Geosci.* 17 (4): 647–659. https://doi.org/10.1007/s10596-013-9346-2.

Wong, J. K.-W. 2018. *Three-dimensional multi-scale hydraulic fracturing simulation in heterogeneous material using Dual Lattice model*. Cambridge, UK: Univ. of Cambridge.

Wrobel, M., G. Mishuris, and P. Papanastasiou. 2021. "On the influence of fluid rheology on hydraulic fracture." *Int. J. Eng. Sci.* 158 (5): 103426. https://doi.org/10.1016/j.ijengsci.2020.103426.

Xie, Y., Y. He, Y. Xiao, and T. Jiang. 2022. "Productivity prediction of multistage fractured horizontal wells in tight oil reservoirs with fully coupled flow and geomechanics." *J. Energy Eng.* 148 (5): 05022002. https://doi.org/10.1061/(ASCE)EY.1943-7897.0000849.

Yang, Y., H. Jiang, M. Li, S. Yang, and G. Chen. 2016. "A mathematical model of fracturing fluid leak-off based on dynamic discrete grid system." *J. Pet. Explor. Prod. Technol.* 6 (3): 343–349. https://doi.org/10.1007/s13202-015-0188-4.

Zhang, K., et al. 2018. "Lateral percolation and its effect on shale gas accumulation on the basis of complex tectonic background." *Geofluids* 2018 (Jan): 5195469. https://doi.org/10.1155/2018/5195469.

Zhou, Y., Y. Jiang, J. Liang, Y. Gu, Y. Fu, and Y. Xiao. 2021. "Reservoir characteristics and major controlling factors of the Cambrian Xixiangchi formation, Central Sichuan Basin, Southwest China." *J. Energy Eng.* 147 (6): 04021051. https://doi.org/10.1061/(ASCE)EY.1943-7897.0000803.

Zielonka, M. G., K. H. Searles, J. Ning, and S. R. Buechler. 2014. "Development and validation of fully-coupled hydraulic fracturing simulation capabilities." In *Proc., SIMULIA Community Conf.* Providence, RI: ExxonMobil Upstream Research Company.

Zolfaghari, N., C. R. Meyer, and A. P. Bunger. 2017. "Blade-shaped hydraulic fracture driven by a turbulent fluid in an impermeable rock." *J. Eng. Mech.* 143 (11): 04017130. https://doi.org/10.1061/(ASCE)EM.1943-7889.0001350.

Zuppann, C., and J. Steinmetz. 2014. *Hydraulic fracturing: An Indiana assessment*. Bloomington, Indiana: Indiana Geological Survey.